12th International Symposium on Turbulence and Shear Flow Phenomena (TSFP12)
Osaka, Japan (Online), July 19-22, 2022

STUDY ON THE CURVATURE OF LAGRANGIAN PARTICLE TRAJECTORIES IN QUANTUM TURBULENCE

Naoto Sakaki
Graduate School of Engineering
Nagoya University
Furo-cho, Nagoya-city, 464-8603, Japan
mw.41g.0347@s.thers.ac.jp

Takumi Maruyama
Graduate School of Engineering
Nagoya University
Furo-cho, Nagoya-city, 464-8603, Japan
takumi.maruyama@a.mbox.nagoya-u.ac.jp

Yoshiyuki Tsuji
Graduate School of Engineering
Nagoya University
Furo-cho, Nagoya-city, 464-8603, Japan
c42406a@nucc.cc.nagoya-u.ac.jp

ABSTRACT

Small particle trajectories are visualized in thermal counterflow using the particle tracking velocimetry technique, and the curvature of two dimensional Lagrangian trajectories are studied. It is found that the probability density function of the curvature demonstrates a power-law tail similar to that of classical turbulence. The curvature distribution is classified into three regions with high, medium, and low values, and the particle velocity is averaged in each region. Furthermore, the particle velocity in the low curvature region clearly shows a bimodal distribution and agrees with the two-fluid model in the case of low heat flux. However, in the high curvature region, the particle velocity deviates from the theoretical value and exhibits a Gaussian distribution.

INTRODUCTION

Quantum turbulence is one of the most important research fields. Thermal counterflow is a simple example of quantum turbulence. In thermal counterflow, the two-fluid velocity of helium4 demonstrates the following relation, when considering mass conservation, $\rho_s v_s + \rho_n v_n = 0$, where ρ and v are fluid density and velocity, respectively. Moreover, the lower subscript n and s represent the superfluid and normal fluid components, respectively. The normal fluid velocity is given by

$$v_n = q/\rho ST \tag{1}$$

with a total density of $\rho = \rho_s + \rho_n$, entropy S, temperature T, and heat flux q. Additionally, the quantum vortices are generated and tangled in turbulent flow in high q.

In recent years, visualization of thermal counterflow has been conducted by several researchers (Paoletti *et al.* (2008); Chagovets & Van Sciver (2011); Kubo & Tsuji (2017); Mastracci & Guo (2018)), using particle tracking velocimetry (PTV). Previous research on thermal counterflow visualization mainly focuses on the velocity and acceleration of the tracer particles in Lagrangian properties. However, the curvature of tracer trajectories has not been studied in detail in thermal counterflow. In classical turbulence, particle acceleration and the curvature of Lagrangian trajectory are analyzed by Xu *et al.* (2007). In magnetic turbulence, the curvature of the magnetic field line is analyzed in a two-dimensional (2D) magneto hydro dynamic (MHD) turbulence (Yang *et al.* (2019)). These investigations revealed that the probability density function (PDF) of curvature has an apparent power-law tail shape.

The thermal counterflow flow characteristics for helium are different from classical turbulence and MHD turbulence. In particular, the PDF varies and often exhibits a bimodal distribution, but the PDF of classical turbulence in homogeneous isotropic turbulence closely resembles a Gaussian distribution. It is also assumed that the Lagrangian trajectories of small particles show different characteristics in quantum and classical turbulence. Trajectory of the particle can rapidly change before and after the particles are trapped by the quantum vortex. Therefore, characterizing this process by geometrical information of curvature is interesting. In addition, other physical quantities, such as velocity can be investigated in the region where the curvature is high for further analysis. Therefore, we aim to determine the particle trajectory features in quantum turbulence when they are conditioned by their curvature.

In this study, we analyzed the motion of solid hydrogen particles in thermal counterflow using the PTV algorithm. Here, we do not classify the particle size because the curvature PDF does not depend on the particle size (Sakaki *et al.* (2022)), although the PDF of vertical velocity depends on the particle size (Kubo & Tsuji (2017)). The relation between the particle velocity and curvature of trajectories is studied by conditional sampling. Moreover, the particle velocity conditioned by high and low curvature regions is compared with the velocity of the two-fluid model. Finally, the interaction between the quantum vortex and the tracer particles is discussed.

EXPERIMENTS

A schematic of the experimental setup is shown in Fig. 1, where the acrylic rectangular channel is set inside the cryostat. The channel cross-section has an area of A $= 20 \times 20$ mm^2 and the height is H $= 260$ mm (Kubo & Tsuji (2017)), and

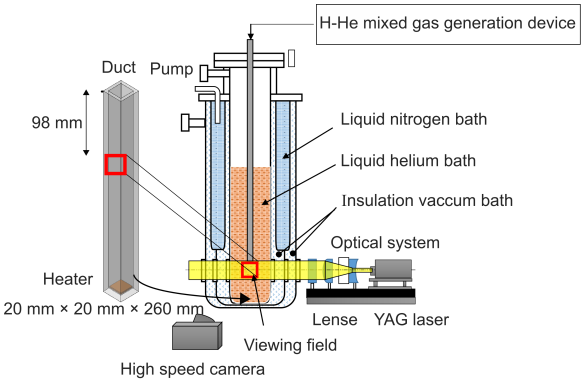

Figure 1. Schematic view of experimental settings.

Table 1. This is an example of a table.

T	q	Number of datasets
1.9 K	≈ 800 W/m^2	11
2.0 K	≈ 300 W/m^2	3
2.0 K	≈ 400 W/m^2	5
2.0 K	≈ 800 W/m^2	13
2.1 K	≈ 800 W/m^2	3

the bath temperature T is varied from 1.9 to 2.1 K. Furthermore, the plate heater is located at the bottom, and the heat flux q is varied in the range of $300-800$ W/m^2. The thermal counterflow is generated inside the channel, and the experimental conditions are listed in Table 1 A high-speed camera(1024×1024 pixels, 8 bit) is used for visualizing the area of 8.7×8.7 mm^2 at 250 fps. A continuous laser (wavelength 532 nm, diode-pumped solid-state laser and 1 W at maximum power) is adopted to make the laser sheet with a thickness of about 1 mm. A helium and hydrogen mixing chamber is designed to vary the mixing ratio and the spouting pressure. The hydrogen particles are generated in the liquid helium. We adopted a mixing ratio of He:H_2 = 40:1 and a spouting pressure 20 kPa. Additionally, the injection is carried out just above the λ point, and then the bath temperature is decreased. In this study, the particle tracking algorithm[1] is employed where the particle size, d, is similar to the previous experiment (Kubo & Tsuji (2019)). It is in the range of $5-40$ μm (Sakaki *et al.* (2022)). In this research, we analyze the motion of all particle sizes, and we do not classify the size of the particles.

ANALYSIS METHOD

The instantaneous curvature can be expressed as $\kappa = a_n/u^2$ (Braun *et al.* (2006)) utilizing the Frenet formulas, where a_n is the magnitude of the normal acceleration, and u is the velocity. The velocity and acceleration are calculated by the numerical derivative with the central difference method. The uncertainly is $O(\Delta t)$ for velocity and $O(\Delta t^2)$ for acceleration.

The distribution of κ has been studied in classical turbulence (Braun *et al.* (2006); Xu *et al.* (2007)). The PDF of κ ($P(\kappa)$) demonstrates the two power-law regions where the high and low curvature regions have corresponding PDFs of $P(\kappa)\propto\kappa^{-5/2}$ and $P(\kappa)\propto\kappa$, respectively. Xu *et al.* (2007) reported that this feature could be understood by the Gaussian property of random variables but not turbulent small-scale statistics. As is well known, the velocity fluctuation in classical turbulence closely mimics the Gaussian property. In addition, the velocity fluctuations (u_x, u_y, u_z) in HIT are independent of one another, then the magnitude $u^2=u_x^2+u_y^2+u_z^2$ should follow a chi-squared distribution with degree of freedom three. When $\kappa\to\infty$, or $u\to0$, the PDF of κ follows the distribution of u^{-2} with the assumption of finite a_n in this limit, suggesting a power-law with an exponent of $-5/2$. Similarly, the power-law scaling of $\kappa\to0$ is derived. The PDF of curvature scales like the PDF of a_n as $a_n\to0$ with the assumption that the components of a_n are independent Gaussian random variables. Then the PDF of a_n^2 then follows a chi-squared distribution with a degree of freedom of two. In the case of $\kappa\to0$, the PDF of κ follows the distribution of a_n as $a_n\to0$, then the power-law with an exponent of one is derived by Xu *et al.* (2007).

Moreover, the PDF of curvature in 2D case is also discussed. Since the PDF of a_n near zero can be approximated as a quasi-Gaussian distribution, then the power-law of PDFs are derived as $P(\kappa)\approx\kappa^{-2}$ and $P(\kappa)\approx\kappa^0$ in $\kappa\to\infty$ and $\kappa\to0$, respectively, using Taylor's expansion.

RESULTS AND DISCUSSION

In Fig. 2, the PDF of the vertical velocity v_y in the case of $T=2$ K with $q=310$ W/m^2 is shown, in which the vertical velocity is normalized by its standard deviation σ. The PDF has a bimodal distribution which is similar to previous studies (Paoletti *et al.* (2008); Mastracci & Guo (2018)). This bimodal distribution is confirmed in almost all cases. The bimodal distribution is approximated by two Gaussian distributions represented by the blue and red dashed lines in Fig. 2. Their mean values are defined as $v_{gauss,s}$ and $v_{gauss,n}$, respectively. The red line is the positive mean value $v_{gauss,n}$ and the velocity v_n is calculated by the two-fluid model (equation (1)), which is indicated by the solid black line. The bimodal distribution was not observed in the case of $T=2.1$ K; however, the positive peak always appears. This was also confirmed by previous study Mastracci *et al.* (2017) for similar heat flux $q\approx900$ W/m^2. The mean velocity $v_{gauss,n}$ was plotted against v_n in Fig. 3. Different colors represent various experimental conditions. Moreover, the solid line is given by $v_{gauss,n}=v_n$, and the dotted line is denoted by $v_{gauss,n}=v_n/2$. There have been discussions on the particle velocity in counterflow (Paoletti *et al.* (2008); Chagovets & Van Sciver (2011)): the previous studies are summarized in Mastracci & Guo (2018). In the previous studies (Paoletti *et al.* (2008); Chagovets & Van Sciver (2011); Mastracci & Guo (2018)), the $v_{gauss,n}$ agrees with v_n. In this measurement, $v_{gauss,n}$ and v_n increase as the heat power becomes large, and $v_{gauss,n}$ locates between v_n and $v_n/2$.

The example PDF of curvature normalized by the standard deviation σ_κ is plotted in Fig. 4 in the case of $T=2.0$ K with $q=470$ W/m^2. In the larger curvature region, the power-law κ^{-2} is observed. On the other hand, in the smaller curvature region, the power-law κ^0 is shown. The PDFs in other cases have the same trend as the case of $T=2.0$ K with $q=470$W/m^2. PDFs of curvature contain no signs of non-classical behavior attributed to the quantum vortex in superfluid. For further analysis, the PDF of the curvature is divided

[1]This was developed by Crocker J. & Weeks E.& Grier D..

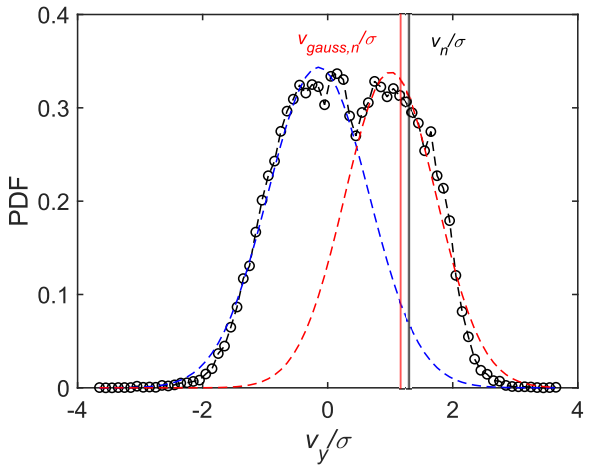

Figure 2. PDF of vertical velocity component for the case of $T = 2$ K with $q = 310$ W/m^2. The bimodal PDF is approximated by two Gaussian profiles denoted by two dashed lines. The solid red line is the mean value v_y, the mean of the positive Gaussian fitting. The solid black line is the normal fluid velocity calculated by the two-fluid model.

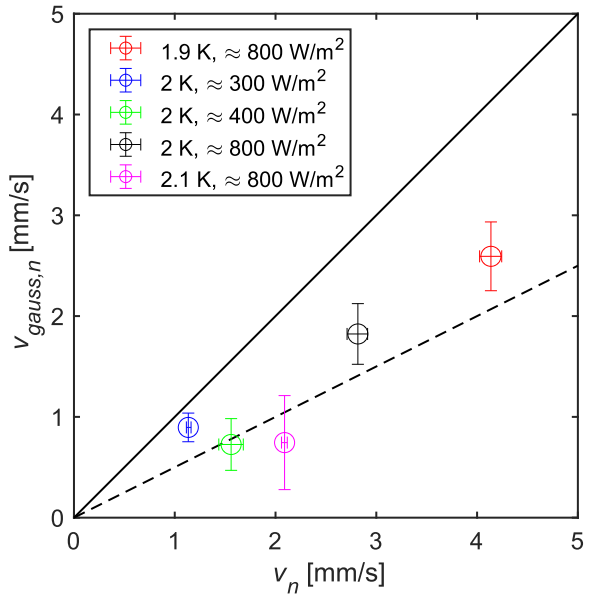

Figure 3. Comparison of mean vertical velocity in experiments and the two-fluid model. The red color is $T = 1.9$ K with $q \approx 800$ W/m^2, blue is $T = 2.0$ K with $q \approx 300$ W/m^2, green is $T = 2.0$ K with $q \approx 400$ W/m^2, black is $T = 2.0$ K with $q \approx 800$ W/m^2, and magenta is $T = 2.1$ K with $q \approx 800$ W/m^2. The vertical error bar is the standard deviation in the each data sets. The horizontal error bar is the range of the theoretical normal fluid in the each data sets. The solid line represents $v_{gauss,n} = v_n$. The dotted line denotes $v_{gauss,n} = v_n/2$.

into three regions: low, medium, and high curvature regions as described in Fig. 5. This classification is defined as the probability that each region is equal for convenience, therefore it does not contain any physical signs. In the low curvature region, the PDF shows flat, or the power law is κ^0, and in the high curvature region, the PDF behaves κ^{-2}. The medium region is located between these two power-law regions. A typ-

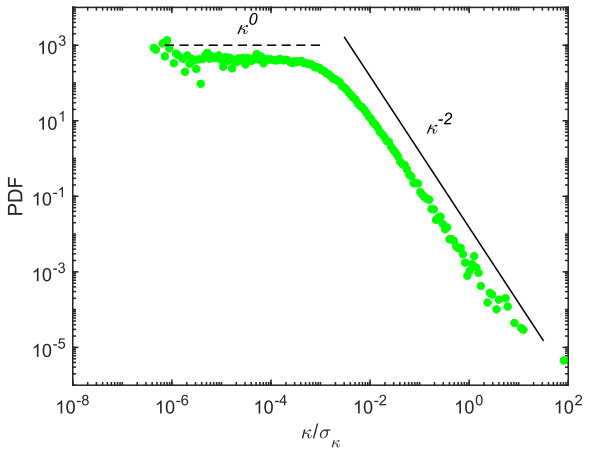

Figure 4. PDF of curvature normalized by the standard deviation is shown in the case of $T = 2.0$ K with $q = 470$ W/m^2. The dotted black line represents the κ^0. The solid black line is given by the κ^{-2}.

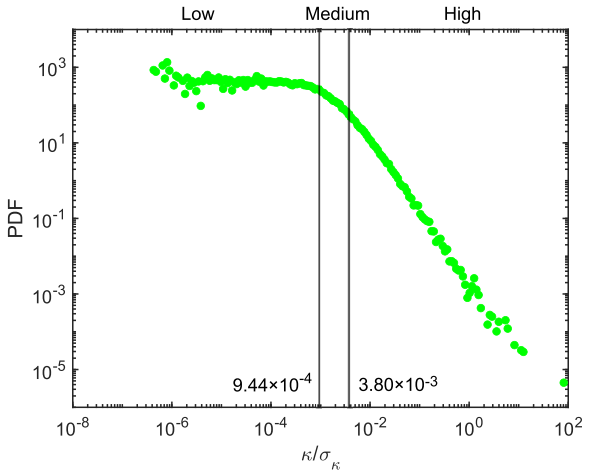

Figure 5. PDF of curvature is divided into the high, medium, and low regions for the $T = 2.0$ K with $q = 470$ W/m^2. Green circles denote the PDF of curvature, the left solid line is the threshold between the low and medium region, and the right solid line is the threshold between the high and medium region.

ical example of the PDF is plotted in Fig. 5, where the low and the high curvature PDFs are given by $\kappa/\sigma_\kappa < 9.44 \times 10^{-4}$ and $3.80 \times 10^{-3} < \kappa/\sigma_\kappa$, respectively. The histogram of particles is plotted in Fig. 6 as a function of curvature and vertical velocity. As described in Fig. 5, the curvature is classified into three regions according to the definition. The histogram indicates the high probability in the medium curvature region where the positive vertical velocity is dominant. Around a small vertical velocity of $v_y \simeq 0$, the high curvature motion is indicated. From these observations, we understand that the vertical velocity has different characteristics depending on the curvature. Then, the vertical velocity is averaged in each curvature region, and it is usually called conditional sampling.

The vertical velocity is divided into high, medium, and low curvature regions, and their PDF is shown in Fig. 7 for the case of $T = 2$ K with $q = 470$ W/m^2. The original PDF shows the bimodal distribution. However, in the velocity conditioned by the low curvature region, there are two more clearly sepa-

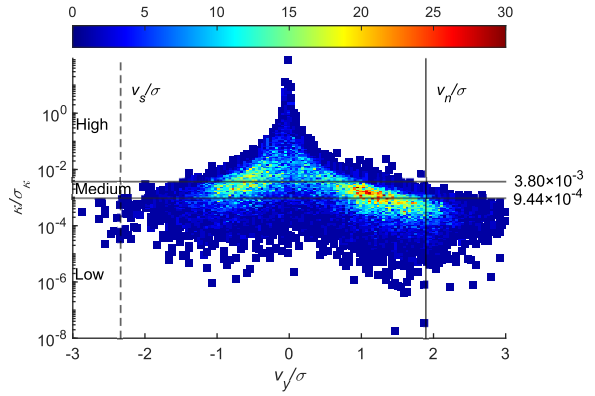

Figure 6. Histogram of particles as a function of y direction velocity and curvature in the case of $T = 2.0$ K with $q = 470$ W/m^2. The lower solid line represents the threshold between the low and medium regions, and the solid upper line signifies the threshold between the high and medium regions. The left dotted line denotes the theoretical superfluid velocity divided by the standard deviation of the vertical velocity and the right solid line is the theoretical normal fluid velocity divided by the standard deviation of the vertical velocity.

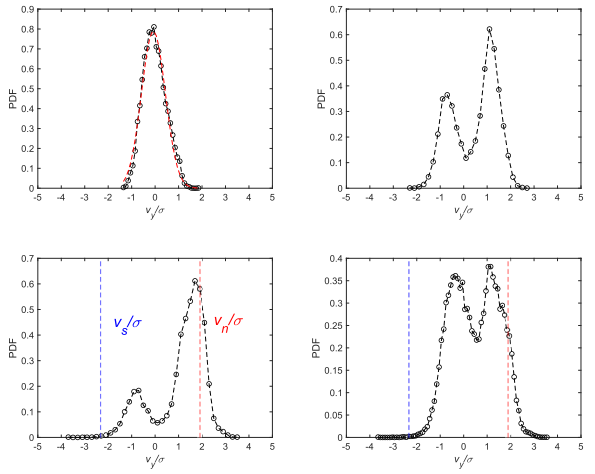

Figure 7. PDF of vertical velocity divided by its standard deviation in high (top left), medium (top right), low (bottom left), and all (bottom right) curvature regions at $T = 2$ K and $q = 470$ W/m^2. In the high region, the dotted orange line represents the Gaussian fit.

rated peaks. The positive peak is given by $v_{gauss,n}/\sigma \simeq 2.0$, and the negative peak is denoted by $v_{gauss,s}/\sigma \simeq -1.0$. In the high curvature region, the profile of the PDF is approximated by the Gaussian distribution. In addition, we found that the horizontal velocity in high curvature region is also approximated by Gaussian distribution (not shown here). Therefore, the magnitude of the velocity $v_x^2 + v_y^2$ follows a chi-squared distribution with a degree of freedom two. When $\kappa \to \infty$, the PDF of κ follows the distribution of $(v_x^2 + v_y^2)^{-2}$ with the assumption of finite a_n in this limit. Therefore, the PDF of curvature has a power-law tail of -2. Similarly, the power-law of κ^0 is assumed because the normal acceleration could be thought of as Gaussian, and the velocity is finite in the limit of $\kappa \to 0$ or $a_n \to 0$.

The positive velocity peak is attributed to the conditional

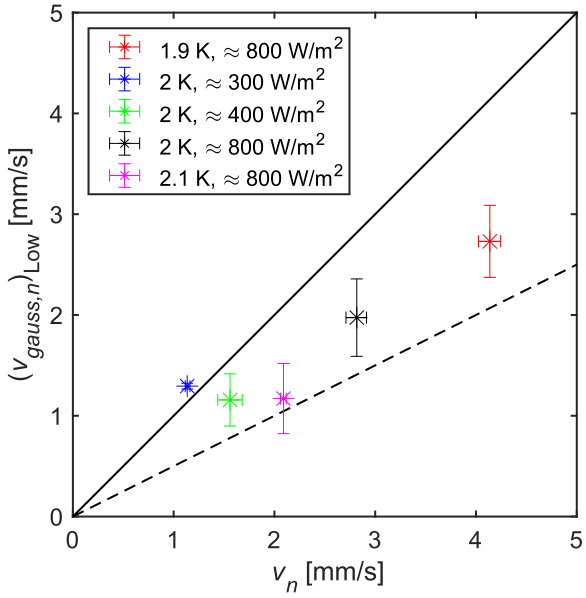

Figure 8. Comparison of mean vertical velocity in experiments and the two-fluid model. The red color is $T = 1.9$ K with $q \approx 800$ W/m^2, blue is $T = 2.0$ K with $q \approx 300$ W/m^2, green is $T = 2.0$ K with $q \approx 400$ W/m^2, black is $T = 2.0$ K with $q \approx 800$ W/m^2, and magenta is $T = 2.1$ K with $q \approx 800$ W/m^2. The vertical error bar is the standard deviation in the each data sets. The horizontal error bar is the range of the theoretical normal fluid in the each data sets. The solid line represents $v_{gauss,n} = v_n$. The dotted line denotes $v_{gauss,n} = v_n/2$.

velocity in the medium curvature region but is only slightly affected by high curvature regions. The values of the negative peak $v_{gaussu,s}$ are also different depending on the curvature. In addition, negative and positive distributions are enhanced compared with the original PDF because, in the low heat flux, particles that feel stokes drag do not interact with vortices frequently and sometimes go down with quantum vortices. In the high heat flux, the PDF of the vertical velocity conditioned by the low curvature region doesn't have clear bimodal distribution, although the original PDF has a bimodal distribution. The tracer particles tend to move fast enough to detrap from the quantum vortices. Thus, the lower peak is located around the small positive value, and the vertical velocity PDF conditioned by the low curvature region does not have clear bimodal distribution for the high heat flux.

The vertical velocity calculated by the two-fluid model is plotted in Fig. 7. Additionally, the normal fluid velocity $v_{gaussu,n}$ agrees with v_n. Then the low curvature region along the Lagrange trajectory represents the laminar flow region where the particles are carried by Stokes drag. The negative particle velocity $v_{gaussu,s}$ is close to v_s compared with original PDF, however it does not agree with the two-fluid model.

In Fig. 8, the vertical velocity $(v_{gaussu,n})_{\mathrm{Low}}$ conditioned by the low curvature region is plotted against v_n by the $*$ symbol. Furthermore, conditional normal fluid velocities are close to those of the two-fluid model in the case of $v_n < 2$ mm/s. However, the conditional velocity still deviates from the original v_n in high-velocity regions. In Fig. 9, we calculate the difference $(v_{gaussu,n})_{\mathrm{Low}} - v_{gauss,n}$. Note that the data at $T = 2.1$ K with $q \approx 800$ W/m^2 is not included here because bimodal distribution is not shown in this condition. It is found that the difference is large in $v_n < 2$ mm/s but small for

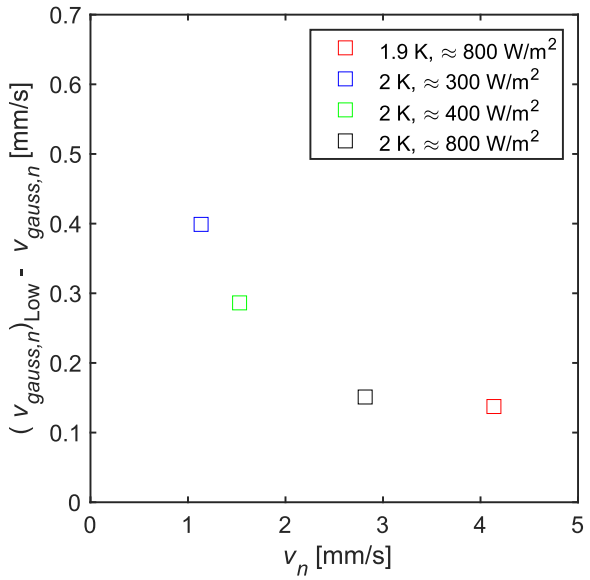

Figure 9. Each squares represent difference between the mean value of Fig. 3 and Fig. 8. The color is the same with that of Fig. 3.

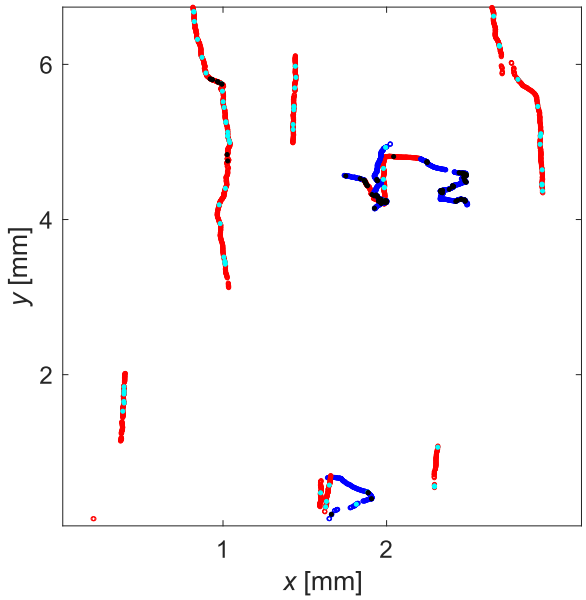

Figure 10. An example of high curvature points on the trajectories for the case of $T = 2.0$ K with $q = 470$ W/m^2. Red and blue trajectories represent the upward and downward motion in the average, respectively. Black points indicate the high curvature region, $7.0 \times 10^{-2} < \kappa/\sigma_\kappa$. Cyan points are the low curvature region, $\kappa/\sigma_\kappa < 4.0 \times 10^{-5}$.

$v_n > 2$ mm/s. Since the quantum vortex density L increases as the heat flux increases, the interaction between the tracer particles and quantum vortices frequently occurs. Thus, the zigzag pattern is shown in the particle trajectories. Moreover, the vertical velocity PDF conditioned by the low curvature region tends to include these velocity components. Therefore, the difference between the PDF of original and low curvature region is small in the high heat flux.

We plot the examples of the high curvature points on the trajectories for $T = 2.0$ K with $q = 470$ W/m^2 in Fig. 10. In Fig. 10, the red and blue points represent the upward and downward motion in the average, respectively. Along the trajectory, the high ($7.0 \times 10^{-2} < \kappa/\sigma_\kappa$) and low ($\kappa/\sigma_\kappa < 4.0 \times 10^{-5}$) curvature region are colored in black and cyan, respectively. As expected, the high curvature region indicates nonstraight motion or the point where the particle motion suddenly changes its direction, which could be due to the quantum vortex interaction. On the other hand, the low curvature region represents the points on almost straight lines.

CONCLUSION

In this study, we calculate the curvature of the 2D-Lagrangian trajectory in thermal counterflow using PTV. The Lagrange velocities (vertical component v_y) are conditionally averaged by curvature. By removing the high curvature region and conditioning the vertical velocity in the low curvature region, we obtain a bimodal velocity distribution, then the normal fluid velocity is close to the value of the two-fluid model. Therefore, the quantum vortex which shows tangled complex interactions are sufficiently separated based on the curvature in the low heat flux case. However, in the high heat flux condition, bimodal distribution does not appear in the low curvature region although it is seen in the original distribution. Both v_y and v_x have a Gaussian distribution with a zero-mean value in the high curvature region. Based on this experimental evidence, we can understand that the PDF of the curvature has power-law scaling $\approx \kappa^{-2}$ in the high curvature region, and is confirmed in the present experiment.

This work was supported by JSPS KAKENHI Grant Number 19H00747. The author N. S. would like to take this opportunity to thank the “Interdisciplinary Frontier Next-Generation Researcher Program of the Tokai Higher Education and Research System.”

REFERENCES

Braun, W., Lillo, F. De & Eckhardt, B. 2006 Geometry of particle paths in turbulent flows. *Journal of Turbulence* **7**, N62.

Chagovets, T. V. & Van Sciver, S. W. 2011 A study of thermal counterflow using particle tracking velocimetry. *Physics of Fluids* **23**, 107102.

Kubo, W. & Tsuji, Y. 2017 Lagrangian Trajectory of Small Particles in Superfluid He II. *Journal of Low Temperature Physics* **187**, 611.

Kubo, W. & Tsuji, Y. 2019 Statistical Properties of Small Particle Trajectories in a Fully Developed Turbulent State in He-II. *Journal of Low Temperature Physics* **196**, 170.

Mastracci, B. & Guo, W. 2018 Exploration of thermal counterflow in He II using particle tracking velocimetry. *Physical Review Fluids* **3**, 063304.

Mastracci, B., Takada, S. & Guo, W. 2017 Study of Particle Motion in He II Counterflow Across a Wide Heat Flux Range. *Journal of Low Temperature Physics* **187**, 446.

Paoletti, M. S., Fiorito, R. B., Sreenivasan, K. R. & Lathrop, D. P. 2008 Visualization of Superfluid Helium Flow. *Journal of the Physical Society of Japan* **77**, 111007.

Sakaki, N., Maruyama, T. & Tsuji, Y. 2022 Statistics of the Lagrangian Trajectories’ Curvature in Thermal Counterflow (in press). *Journal of Low Temperature Physics* .

Xu, H., Ouellette, N. T. & Bodenschatz, E. 2007 Curvature of Lagrangian Trajectories in Turbulence. *Physical Review Letters* **98**, 050201.

Yang, Y., Wan, M., Matthaeus, W. H., Shi, Y., Parashar, T. N.,

Lu, Q. & Chen, S. 2019 Role of magnetic field curvature in magnetohydrodynamic turbulence. *Physics of Plasmas* **26**, 072306.